



PCCP

Ultrafast Electron Transfer at the Interface of Gold Nanoparticles and Methylene Blue Molecular Adsorbates

Journal:	<i>Physical Chemistry Chemical Physics</i>
Manuscript ID	CP-ART-06-2022-002568.R1
Article Type:	Paper
Date Submitted by the Author:	26-Jun-2022
Complete List of Authors:	Contreras, Dillon; California State University Northridge Yuson, Joie; California State University Northridge, Chemistry and Biochemistry Eroglu, Zeynep; California State University Northridge, Chemistry&Biochemistry Bahrami, Pouya; California State University Northridge, Chemistry and Biochemistry Sadeghi Hadad zavareh, Hoda; California State University Northridge Boulesbaa, Abdelaziz; California State University Northridge, Chemistry & Biochemistry

SCHOLARONE™
Manuscripts

ARTICLE

Ultrafast Electron Transfer at the Interface of Gold Nanoparticles and Methylene Blue Molecular Adsorbates

Received 00th June 20xx,
Accepted 00th XXXX 20xx

DOI: 10.1039/x0xx00000x

Dillon Contreras, Joie M. Yuson, Zeynep E. Eroglu, Pouya Bahrami, Hoda Sadeghi Hadad zavareh, and Abdelaziz Boulesbaa*

Due to their unique property of possessing localized surface plasmon resonance (LSPR), metal nanoparticles (MNPs) have drastically impacted many applications. For instance, local field enhancement through LSPRs and plasmonic hot electron transfer are known to enhance the efficiency of MNP-based photoreactions. Here, we report on the ultrafast electron transfer from gold nanoparticle (Au-NPs) to methylene blue (MB) molecular adsorbate using femtosecond pump-probe and steady-state absorption and emission spectroscopy techniques. Although the energy band alignment of the interface allows both dipole-dipole Förster resonance energy transfer (FRET) and charge transfer, because the MB emission intensity at the Au-NPs/MB nanocomposite decreased by a factor of ~ 3.6 , the FRET process was ruled out. Selective excitation of LSPRs at the Au-NPs/MB nanocomposite sample in pump-probe experiments led to the formation of the MB ground-state depletion and an induced absorption at wavelengths shorter than ~ 500 nm, which was attributed to the shoulder of the MB⁻ anion absorption. Furthermore, despite the fact that the concentration of Au-NPs in the nanocomposite sample is the same as that in the Au-NPs solution, the initial intensity of the LSPR depletion signal was about six times weaker than that in the Au-NPs sample. These observations suggest that electron transfer from excited Au-NPs to MB adsorbates took place on a time-scale that is shorter than the ~ 50 fs experimental temporal resolution.

Introduction

The beating heart of metal nanoparticles (MNPs) is their localized surface plasmon resonance (LSPR), which is a collective oscillation of surface conduction band (CB) electrons. Due to the nanoscale quantum confinement of MNPs, one can tailor their LSPRs to specific needs [1, 2]. This excellent property has made LSPRs highly suitable in various applications ranging from photodetection [3], photocatalysis [4], photovoltaics [5, 6], to integrated quantum information science [7]. Upon resonant photoexcitation of MNPs, excited LSPRs rapidly relax via two pathways: a radiative decay process by emitting photons, and a non-radiative channel by creating hot electron-hole pairs via Landau damping on a sub-100 fs time-scale [8-12]. These highly energetic hot electrons rapidly transfer their energy to the thermal equilibrium electrons through electron-electron scatterings on a sub-100 fs time-scale, followed by electron-phonon cooling within a few ps, and heat dissipation from the MNPs to the environment through phonon-phonon scatterings during 100s of ps [13-15]. Radiative decay of LSPRs is beneficial for local field enhancement-based applications, such as light emitting devices and ultrafast photo-switching [16], and the Landau damping process is useful in applications where electron transfer is needed, such as in

photodetection and photocatalysis [17]. Despite the challenging requirement of transferring LSPR electrons and/or energy before their relaxation, several efforts have been successful [18]. For instance, visible pump/infrared probe studies reported that hot electron transfer from gold (Au) nanodots to TiO₂ nanocrystal takes place on a time-scale on the order of ~ 240 fs with $\sim 40\%$ yield [19]. Also, electron transfer from Au₂₅ clusters to pyrene has been reported to happen on a ~ 500 fs time-scale [20]. Furthermore, the presence of Au-NPs in Ag-NWs@TiO₂ core-shell nanocomposite has been reported to promote hot carrier transfer due to a plasmonic coupling effect [21]. Additionally, transient absorption spectroscopy and photocatalytic action spectrum measurements carried out on Au/SiO₂/Cu₂O sandwich nanostructure, indicated that dipole-dipole Förster resonance energy transfer (FRET) from Au to Cu₂O happens on a sub-100 fs time-scale [22].

Recent studies of interfaces involving MNPs and methylene blue (MB) molecular adsorbates using surface-enhanced Raman scattering (SERS) technique have attributed the observed photoinduced chemical transformations to hot electron transfer to MB [23-25]. Here, we incorporate femtosecond transient absorption and steady-state absorption and emission spectroscopies to report on the ultrafast electron transfer from ~ 40 nm-diameter Au-NPs to MB molecular adsorbates. Selective excitation of Au-NPs in the Au-NPs/MB nanocomposite in transient absorption experiments led to a six-fold decrease in the initial amplitude of the LSPR depletion signal, accompanied with a formation of the MB ground-state depletion. These observations

Department of Chemistry & Biochemistry, California State University, Northridge, 18111 Nordhoff Street, Northridge, 91330 CA, USA.

*Author to whom correspondence should be addressed: aboules@csun.edu

are attributed to the transfer of excited electrons from Au-NPs to MB adsorbates on a time-scale that is shorter than the experimental temporal resolution of ~ 50 fs. Furthermore, although dipole-dipole FRET process is allowed based on the alignment of energy levels of the interface, it is ruled out because the MB emission intensity decreased more than three times in the nanocomposite sample compared to that in the MB aqueous sample. These results shed more light on the ultrafast dynamics of plasmonic charge transfer to organic molecules, which is beneficial for the incorporation of MNPs in dye-sensitized solar-cells to enhance the solar-to-electricity conversion efficiency [26].

Materials and Methods

Subject material. Commercial Au-NPs (nanospheres of ~ 40 nm size) dissolved in deionized water and MB powder are purchased from nanoComposix and Sigma-Aldrich, respectively. To prepare the Au-NPs/MB nanocomposite, the stock solution of Au-NPs is divided into two samples, and the MB powder is added to one of them and sonicated for five minutes. To maintain the concentration of Au-NPs in the Au-NPs/MB sample the same as that in the Au-NPs solution, the Au-NPs/MB mixture is diluted using the Au-NPs stock solution. A control sample of MB dissolved in deionized water is made with the same concentration of that in the Au-NPs/MB sample.

Spectroscopy Methods

Femtosecond pump-probe measurements. A detailed description of the femtosecond pump-probe experimental setup has been previously reported [27, 28]. Briefly, it is based on a Titanium:Sapphire femtosecond amplifier (Astrella, Coherent Inc), which provides pulses centred at ~ 800 nm, ~ 35 femtosecond duration, and 6 W average power at a repetition rate of 5 kHz. A small portion of the amplifier's output is focused on a 2-mm thick sapphire window to generate a spectrally broad (480-920 nm) white light supercontinuum (WL) probe. To minimize the optical chirp in the spectrally broad WL probe, a reflective parabolic mirror is used for collimation, and a reflective filter (which transmits 800 nm and reflects other wavelengths) is used for the filtration of the 800 nm fundamental laser. Excitation pump at 400 nm is generated in a 0.5 mm thin beta barium borate (BBO) crystal by frequency-doubling the 800 nm fundamental laser. This frequency doubling is done without focusing and collimating lenses to maintain the pulse ultrashort duration, and the residual 800 nm is rejected through a short-pass filter. The 580 nm excitation pump is generated by frequency-doubling in a BBO crystal the near infrared signal output of an optical parametric amplifier (OPA), which is a TOPAS Prime by Coherent Inc.

The pump and probe beams are brought collinearly into a home-built inverted-upright hybrid microscope based on an Olympus IX71, using various thin (0.5 mm thickness) dichroic filters (which transmit the WL probe and reflect the pump). The collinear pump and probe beams are focused on the sample using a calcium fluoride (CaF_2) lens with 35 mm focal length that is mounted on the microscope nosepiece. After the sample, the two beams are collimated using a second CaF_2 lens, and the pump is filtered out. The collimated WL probe exiting the microscope is focused onto a

100 μm slit entrance of a spectrograph (Horiba iHR320), which is coupled with a CCD (Newton, Andor) equipped with an electron multiplier (EM). To cancel out long-term laser fluctuations, the pump beam passes through an optical chopper set to a 50 Hz frequency, and at every time-delay, the absorbance change is calculated between every 50 successive laser shots. In every experiment, six scans over the covered time-delay range are averaged. The instrument response function (IRF) is measured by cross-correlating the pump and probe pulses in a 100 μm thin film of vanadium oxide (VO_2) on a sapphire substrate, and suggesting a temporal resolution on the order of ~ 50 fs. In all 400 nm-pump/probe experiments, the pump density is kept the same at ~ 8 $\mu\text{J}/\text{cm}^2$. Liquid samples are poured in a 10 \times 10 mm square well with a 2 mm depth, drilled in a 25 \times 25 mm quartz window then covered with a second flat window of 1 mm thickness. The two windows are mounted on a customized aluminium sample holder that is placed horizontally on the microscope motorized XY stage. While the polarization of the pump pulse is parallel to sample's plane, the polarization of the WLC probe is mixed at the sample and detection.

Steady-state absorption and emission. The home-built upright-inverted microscope is equipped with a tungsten halogen light source (HL-2000-LL Ocean Optics) used for measuring the steady-state absorption from the same spot on the sample studied in pump-probe experiments. The detection system used for steady-state absorption and emission studies is the same as that for pump-probe measurements

Results and discussion

In order to evaluate the possibility of achieving charge and/or energy transfers at the interface of Au-NPs and MB adsorbates, we depict in **Figure 1a** the energy band alignment of the interface. The highest occupied molecular orbital (HOMO) and the lowest unoccupied molecular orbital (LUMO) energy levels of MB are reported to be at ~ -6.26 eV and ~ -4.5 eV, respectively [29]. The Fermi energy level of bulk Au is reported to be ~ -5.1 eV [30], and it shifts to ~ -4 eV for NPs (supported on titanium dioxide) of ~ 4 nm diameter with a slight dependence on the NP size where it increases by ~ 3 meV when the size of the particle increases to ~ 13 nm [31]. Since Au-NPs used in this work have a diameter of ~ 40 nm, one may consider that their Fermi level is even higher than -4 eV. Based on this energy diagram, electron transfer from excited LSPRs in Au-NPs to the LUMO level of the MB adsorbate is possible.

The steady-state absorption spectra of Au-NPs, Au-NPs/MB, and MB in water are shown in **Figure 1b**. We started by dividing the Au-NP stock solution into two samples, then we added to one of them MB powder to guarantee that the concentration of Au-NPs is the same in both samples. To adjust the MB concentration, the nanocomposite sample is diluted using the Au-NPs stock solution. The spectra of both samples contain the LSPR peak centred around 520 nm. Also shown in **Figure 1b** is the absorption spectrum of MB aqueous solution (blue solid plot), which contains a main peak around 660 nm and a shoulder peak around 610 nm, which is assigned to vibronic subband and residual dimer absorption [32-34]. To verify that MB in the Au-NPs/Au nanocomposite is not

aggregating, the spectrum of the Au-NPs sample is subtracted from that of Au-NPs/MB nanocomposite, and the resulting spectrum is similar to that of the MB aqueous solution with the exception of a small reduction in absorption around the dimer's peak (~ 610 nm).

To confirm that MB molecules are not aggregating in the presence of Au-NPs, photoluminescence measurements are carried out. Shown in **Figure 1c** are the steady-state emission spectra collected upon excitation at ~ 580 nm of MB and Au-NPs/MB samples. We note that based on the absorption spectra shown in **Figure 1b**, both MB and Au-NPs absorb at ~ 580 nm, and based on the spectral overlap of the two components of the nanocomposite, dipole-dipole FRET is possible [35]. Although the MB emission spectra have identical shapes, which suggests that MB adsorbates are not aggregating, the emission intensity in the case of Au-

NPs/MB sample is more than three times weaker than in the case of the MB aqueous sample; and it is blue shifted by ~ 5 nm due to the change in the dielectric environment. The decrease in the MB emission intensity suggests that charge transfer from Au-NPs to MB has occurred. Injecting electrons to the LUMO level of the MB adsorbates, leads to the formation of MB anions (MB^-), and in an ensemble photoluminescence measurement, the MB emission intensity decreases. Furthermore, if energy transfer from excited Au-NPs to MB has occurred (or at least if it is the dominating process), one expects the MB emission collected from Au-NPs/MB sample to increase, but since it decreased by a factor of ~ 3.6 , we conclude that energy transfer is at least not the dominant process at the studied nanocomposite.

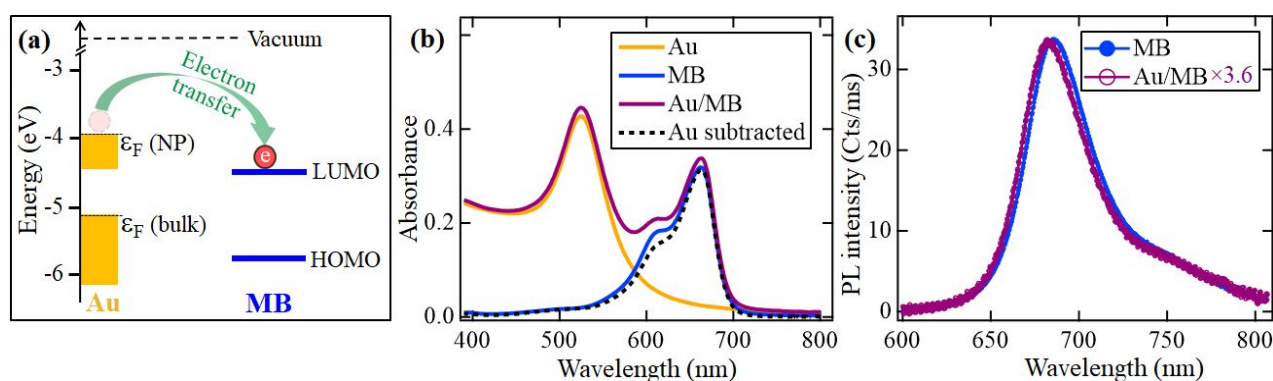


Figure 1. (a) A schematic of the mechanism of electron transfer from excited Au-NPs to MB adsorbates. The values of HOMO and LUMO levels of the MB molecule [29] and the Fermi level for bulk Au [30] and Au-NPs [31] are adopted from previous reports. (b) Steady-state absorption spectra of Au, MB, and Au/MB aqueous samples as indicated. The dashed line is a spectrum obtained by subtracting the Au absorption spectrum from that of Au/MB. (c) Emission spectra of MB with and without Au-NPs following excitation at 580 nm. The spectrum measured from the Au-NPs/MB sample is magnified 3.6 times for a better visual comparison.

The strategy for confirming electron transfer from Au-NPs to MB adsorbates and measuring its dynamics consists of selectively exciting Au-NPs in the Au-NPs/MB nanocomposite sample and compare the resulting spectral and dynamical features to those measured at the Au-NPs sample.

The spectral and dynamical features of the Au-NPs aqueous solution, recorded up to 100 ps time-delays following excitation of the Au-NPs sample at ~ 400 nm, are shown in **Figure 2a**. Transient spectra at a few time-delays are shown in **Figure 2d**. These spectra contain a negative band centred around 525 nm overlapping with a positive band. According to the steady-state absorption spectrum of Au-NPs shown in **Figure 1b**, the negative band is attributed to the depletion of the LSPR transition, and the positive band is assigned to the excited-state induced absorption.

To investigate a possible charge transfer from Au-NPs to MB molecular adsorbates, the Au-NPs/MB nanocomposite is excited with the same pump (photon energy and density) as the Au-NPs sample, and the resulting transient absorption traces recorded up to 100 ps time-delay are shown in **Figure 2b**. Transient spectra at a few time-delays are shown in **Figure 2e**. A visual comparison of these results to those measured at the Au-NPs sample shown in **Figures 2a** and **2d** indicates that the LSPR depletion peak center shifts from ~ 524 nm in the case of the Au-NPs sample to ~ 528 nm

in the case of the Au-NPs/MB sample. This is expected because adsorbing MB molecules at the surface of Au-NPs affects their optical properties as it has been reported previously [36]. Furthermore, three additional distinctions are as follows:

i) Despite that both samples have the same concentration of Au-NPs and both experiments are carried out using the same pump photon-energy and density, the amplitude of the LSPR depletion signal (around 525 nm) is about six times weaker than that in the case of the Au-NPs sample.

ii) The amplitude of the induced absorption signal (around 490 nm) is about 80% to that of the LSPR depletion signal, whereas in the case of the Au-NPs sample, it was less than 25% to that of the LSPR depletion signal.

iii) The spectra contain, in addition to the LSPR depletion and the induced absorption signals, two weak negative bands around 580 nm and 660 nm.

According to the steady state-state absorption spectrum of MB shown in **Figure 1b**, we assign these weak negative signals observed around 580 and 660 nm to the depletion of the MB ground state absorption. We note that the negative high-energy band around 580 nm is blue-shifted compared to the steady state spectrum shown in **Figure 1b** where it occurs at ~ 610 nm, suggesting some

dimerization of MB adsorbates, which is consistent with previous reports that indicated dimerization of MB at charged interfaces [37, 38]. Based on the steady-state absorption spectrum of the MB sample shown in **Figure 1b**, an excitation around 400 nm of the Au-NPs/MB nanocomposite should not lead to an excitation of the MB molecular adsorbates, and consequently, a depletion of the MB ground-state transition should not be observed. To confirm this, we excited the MB aqueous solution, which has the same concentration as that of MB in the nanocomposite sample as shown in **Figures 1b**, and with the same pump (photon energy and density) as in the case of the transient absorption experiment carried on the nanocomposite sample. The results shown in **Figures 2c** and **2f** indicate that under these conditions (MB concentration, pump

photon-energy, and pump density), no depletion of the MB ground-state transition is observed. Consequently, one can conclude that the depletion of the MB ground-state transition observed in **Figures 2b** and **2e** for the nanocomposite sample is likely due to electron transfer from excited LSPRs of Au-NPs to MB adsorbates. We note that upon charge transfer, the MB adsorbate is reduced and will no longer be in its neutral ground-state, and a depletion of the ground-state transition is observed in a pump-probe experiment [35]. We note that although the observed MB ground-state depletion signal can be caused by energy transfer from excited LSPRs to MB as well, because we excluded this possibility in the discussion of emission results (or at least minimized its likelihood), we limit the discussion of transient absorption results to the possibility of electron transfer.

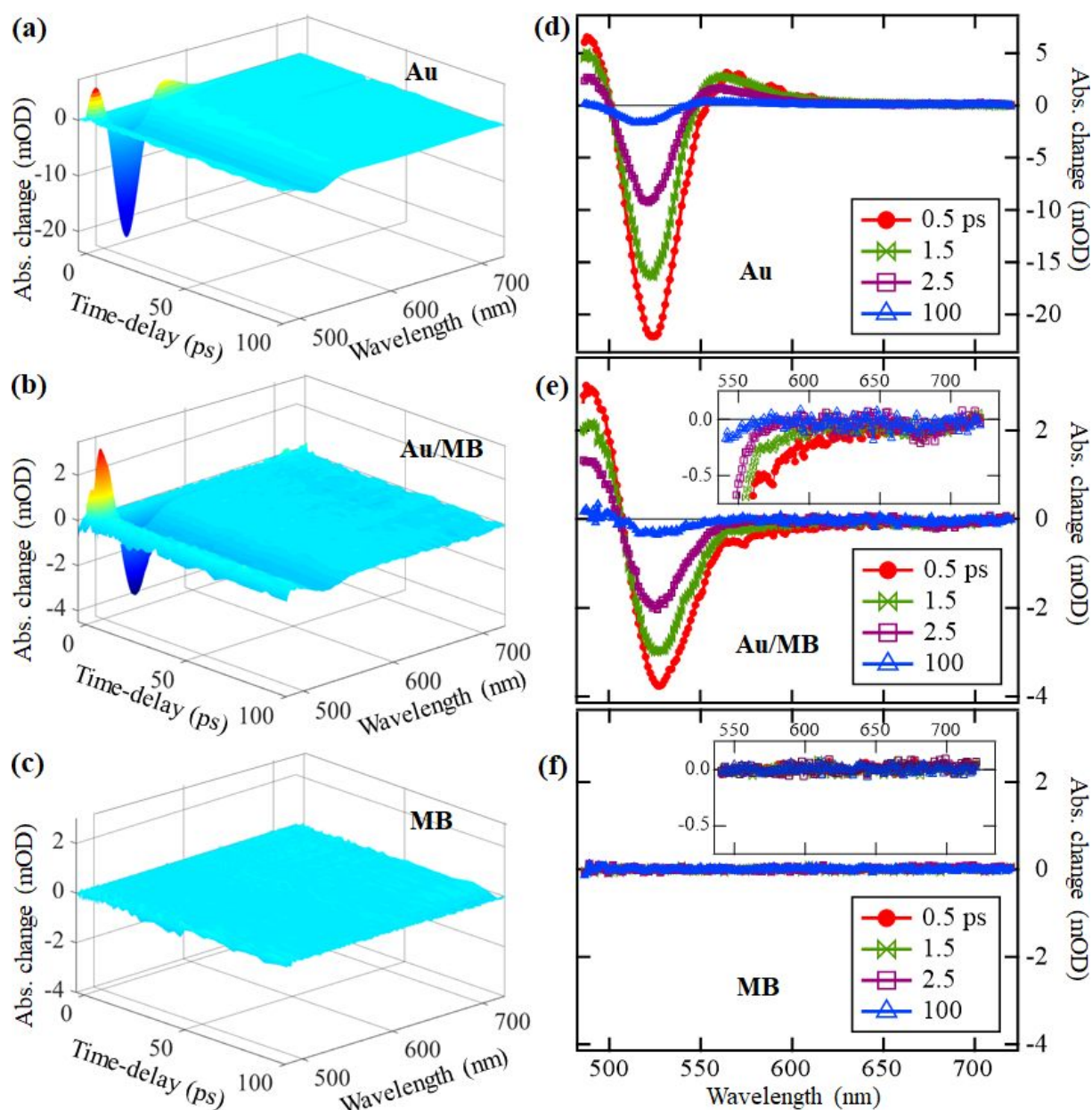


Figure 2. Transient absorption traces recorded up to 100 ps following excitation at ~ 400 nm of aqueous samples (a) Au-NPs, (b) Au-NPs/MB, and (c) MB. Transient spectra recorded at the indicated time-delays for samples (d) Au-NPs, (e) Au-NPs/MB, and (f) MB. The insets in (e) and (f) are amplitude-zooms around the indicated wavelength range.

To shed more light on the investigation of electron transfer from Au-NPs to MB molecular adsorbates, we compare the LSPR depletion dynamics measured at the Au-NPs sample and the MB ground-state depletion measured at the MB aqueous sample to those measured at the Au-NPs/MB nanocomposite. The results are shown in **Figure 3**. We fitted the LSPR depletion dynamics to a multiexponential decay function convoluted with the IRF. Because the LSPR depletion signal (negative amplitude around 525 nm) and

the excited-state induced absorption (positive amplitude around 490 nm) are overlapping, when fitting the dynamics of each signal, we included one component with opposite amplitude sign to account for the effect of the other signal. The returned fit parameters are list in **Table 1**.

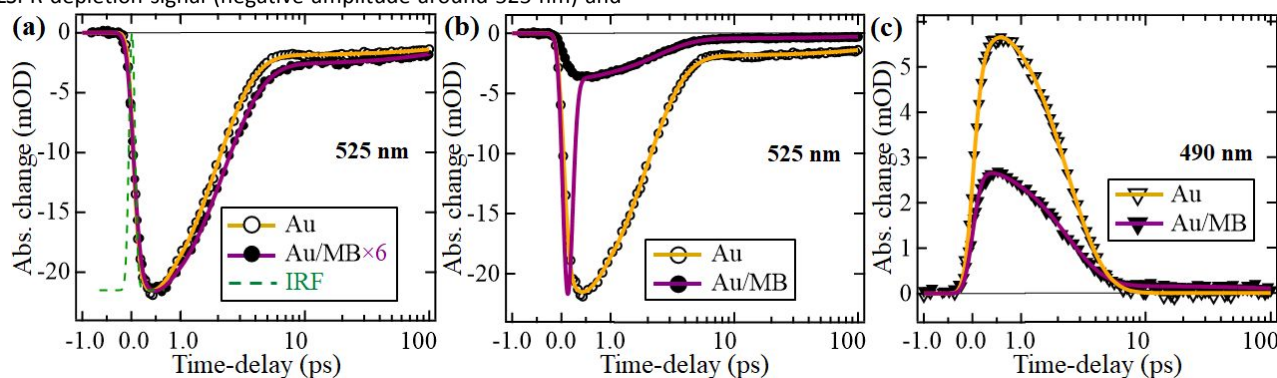


Figure 3. (a) LSPR depletion dynamics averaged around 525 nm. (b) Same as in (a) but the fit is forced to consider the initial amplitude of the signal in the case of the nanocomposite sample equal to that in the case of Au-NPs sample. (c) Dynamics of the induced absorption averaged around 490 nm. Solid plots are fits to a multiexponential decay function convoluted with the IRF. Time-delay axes are plotted in a linear scale up 1 ps time-delay, and in a logarithmic scale thereafter.

Shown in **Figure 3a** are the dynamics of LSPR depletion signal measured from the Au-NPs and Au-NPs/MB samples. In the case of the nanocomposite, the signal is magnified six times for a better visual comparison. In the case of the Au-NPs sample, the majority of the LSPR excited population decays with a time-constant of ~ 1.1 ps, and the remaining population decays with a time-constant of ~ 333 ps. The fast component is assigned to electron-electron scattering and electron-phonon relaxation, which have been reported to take place on sub-ps and a few ps time-scales, respectively [13, 14]. The slow component is attributed to phonon-phonon relaxations [13, 14]. Although the LSPR depletion recovery dynamics in the nanocomposite sample seem faster compared to those measured at the Au-NPs sample, the importance of the signal amplitude needs careful consideration. Because the two samples are excited with the same pump wavelength and density, and since they both contain the same concentration of Au-NPs, the amplitude of the LSPR depletion signal should be the same in both samples. The fact that the LSPR depletion signal measured from the Au-NPs/MB nanocomposite is six times weaker than that observed at the Au-NPs sample suggests that the “missing” amplitude is due to electron transfer to MB adsorbates. We hypothesize that because the electron transfer is faster than the temporal resolution of the experiment, the dynamics at early time-delays are not captured. When we forced the fit of the LSPR depletion in the case of the Au-NPs/MB sample to consider the initial amplitude equal to that in the case of the Au-NPs sample as shown in **Figure 3b**, the fit required an additional decay component with a time-constant of ~ 24 fs (component 4 in **Table 1**). We recognise that this analysis does not reveal the real electron transfer time, but it only suggests that the electron transfer time is faster than the experimental

temporal resolution. We note that a plasmonic electron transfer from silver (Ag) NPs to silver chloride cubic cages (AgCl) faster than the experimental temporal resolution has been reported [39].

Shown in **Figure 3c** is a comparison of the dynamics around 490 nm. In the case of the Au-NPs sample, by the 10 ps time-delay, the signal completely decayed to zero and it required only one exponential decay component with a time-constant of ~ 1.2 ps. However, in the case of the nanocomposite sample, the dynamics required a second exponential decay component with a time-constant of ~ 227 ps to account for the remaining excited population beyond the ~ 10 ps time-delay. We note that the amplitude, and thus the population, of the slow component is almost negligible ($\sim 1/30$) compared to the population decaying with the fast component.

Unlike in the case of the Au-NPs sample where the positive signal at ~ 490 nm originates only from the excited state of LSPRs, in the case of the nanocomposite sample, it has additional possible causes. For instance, according to previous reports, it coincides with the MB excited-state absorption and with the “red” shoulder of the MB $^-$ anion absorption [40, 41]. The contribution of MB excited-state absorption due to direct excitation of MB by the pump can be excluded for the same reasons listed above when we discussed the origin of the observed MB ground-state depletion. However, the contributions of the MB excited-state and/or anion absorptions due to energy and/or charge transfer, respectively, from excited LSPRs to the MB adsorbate are possible.

ARTICLE

Table 1. List of the fit parameters of LSPR excited-state induced absorption (at ~ 490 nm) and depletion (at ~ 525 nm), and the MB ground-state depletion (at ~ 580 nm) in the three studied samples. A_i (mOD) and t_i (ps) are the amplitudes and time constants of the exponential component i . Error bars are standard deviations extracted from the six scans of each experiment.

	490 nm		525 nm		580 nm	
	Au	Au/MB	Au	Au/MB	MB	Au/MB
A_1	-23.8 ± 2.34	-23.7 ± 3.21	$+48.2 \pm 4.53$	$+14.3 \pm 1.87$	-1.28 ± 0.62	-0.72 ± 0.15
t_1	0.84 ± 0.12	1.00 ± 0.23	0.64 ± 0.07	0.98 ± 0.18	2.32 ± 0.36	1.01 ± 0.31
A_2	$+28.3 \pm 3.11$	$+34.4 \pm 2.11$	-65.3 ± 9.47	-17.6 ± 2.07	-0.65 ± 0.13	
t_2	1.20 ± 0.32	1.15 ± 0.32	1.10 ± 0.32	1.25 ± 0.42	278 ± 12.8	
A_3		0.16 ± 0.07	-1.90 ± 0.27	-0.45 ± 0.21		
t_3		227 ± 13.6	333 ± 17.2	250 ± 12.7		
A_4				-205 ± 11.5		
t_4				0.024 ± 0.008		

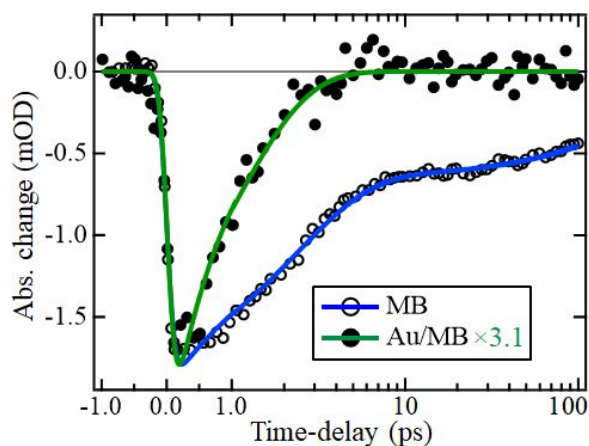


Figure 4. Dynamics of the MB depletion signal averaged around 580 nm following excitation at ~ 400 nm of the Au-NPs/MB nanocomposite sample, and averaged around 610 nm for the MB aqueous sample following excitation at ~ 580 nm. Solid plots are fits to a multiexponential decay function convoluted with the IRF. Time-delay axes are plotted in a linear scale up to 1 ps time-delay, and in a logarithmic scale thereafter.

To decide whether the origin of the observed MB ground-state depletions (at ~ 580 nm and ~ 680 nm) and the positive induced absorption (at wavelengths below 500 nm) is charge transfer or energy transfer, we compared the MB depletion recovery dynamics at the Au-NPs/MB sample to those recorded following a direct excitation at ~ 580 nm of the MB aqueous sample as shown in **Figure 4**. Because the amplitude of the low energy depletion peak

(~ 660 nm) measured at the nanocomposite sample is very weak (~ 0.1 mOD as shown in the inset of Figure 3e), we considered the dynamics of the high-energy band (580–610 nm). The dynamics of the MB ground-state depletion and excited-state induced absorption that form because of energy transfer from Au-NPs should be similar to those measured upon direct excitation of the MB aqueous sample at ~ 580 nm. According to Figure 4 and Table 1, the MB depletion signal in the case of the Au-NPs/MB sample recovers with a time-constant of ~ 1 ps, whereas, upon direct excitation of the MB aqueous sample, the ground-state depletion recovery takes 100's of ps. This suggests that the MB ground-state depletions observed at ~ 580 nm and ~ 660 nm, and the induced absorption observed at ~ 490 nm at the Au-NPs/MB nanocomposite are more likely due to electron transfer than to energy transfer from Au-NPs to MB adsorbates.

Conclusion

In summary, we employed steady-state absorption and emission spectroscopies, and femtosecond transient absorption to investigate electron transfer from Au-NPs to MB molecular adsorbates. Although the energy band alignment of the interface allows both dipole-dipole FRET and charge transfer, because the MB emission intensity at the Au-NPs/MB nanocomposite decreased by a factor of ~ 3.6 , the FRET process was ruled out, or its likelihood was at least minimized. Selective excitation of LSPRs at the Au-NPs/MB nanocomposite in pump-probe experiments led to the formation of the MB ground-state depletion and a positive induced absorption at wavelengths shorter than ~ 500 nm, which was attributed to the shoulder of the MB⁻ anion absorption.

Furthermore, despite the fact that the concentration of Au-NPs in the nanocomposite sample is the same as that in the Au-NPs solution, the initial intensity of the LSPR depletion signal was about six times weaker than that in the Au-NPs sample. These observations suggested that electron transfer from excited Au-NPs to MB adsorbates took place on a time-scale that is shorter than the ~ 50 fs experimental temporal resolution. Capturing the electron transfer dynamics at the MNP/organic molecular adsorbate using a sub-20 fs temporal resolution is our next step for a better understanding of the process, which will be beneficial to the incorporation of MNPs in dye-sensitized solar-cells with enhanced conversion efficiency.

Conflicts of interest

There are no conflicts to declare".

Acknowledgements

The authors acknowledge support from NSF under grant DMR-1828019, and NIH with grant numbers NIGMS RL5GM118975 and TL4GM118977.

References

1. K. A. Willets, R. P. Van Duyne: "Localized Surface Plasmon Resonance Spectroscopy and Sensing". *Annual Review of Physical Chemistry* 2007, **58**:267-297.
2. A. Boulesbaa, V. E. Babicheva, K. Wang, I. I. Kravchenko, M.-W. Lin, M. Mahjouri-Samani, C. B. Jacobs, A. A. Poretzky, K. Xiao, I. Ivanov *et al.*: "Ultrafast Dynamics of Metal Plasmons Induced by 2D Semiconductor Excitons in Hybrid Nanostructure Arrays". *ACS Photonics* 2016, **3**:2389-2395.
3. M. W. Knight, H. Sobhani, P. Nordlander, N. J. Halas: "Photodetection with Active Optical Antennas". *Science* 2011, **332**:702-704.
4. P. Christopher, H. Xin, S. Linic: "Visible-light-enhanced catalytic oxidation reactions on plasmonic silver nanostructures". *Nature Chemistry* 2011, **3**:467-472.
5. H. A. Atwater, A. Polman: "Plasmonics for improved photovoltaic devices". *Nature Materials* 2010, **9**:205-213.
6. S. Mubeen, J. Lee, N. Singh, S. Krämer, G. D. Stucky, M. Moskovits: "An autonomous photosynthetic device in which all charge carriers derive from surface plasmons". *Nature Nanotechnology* 2013, **8**:247-251.
7. B. J. Lawrie, P. G. Evans, R. C. Pooser: "Extraordinary Optical Transmission of Multimode Quantum Correlations via Localized Surface Plasmons". *Physical Review Letters* 2013, **110**:156802.
8. L. M. Brongersma, N. J. Halas, P. Nordlander: "Plasmon-induced hot carrier science and technology". *Nature Nanotechnology* 2015, **10**:25-34.
9. C. Clavero: "Plasmon-induced hot-electron generation at nanoparticle/metal-oxide interfaces for photovoltaic and photocatalytic devices". *Nature Photonics* 2014, **8**:95-103.
10. X. Li, D. Xiao, Z. Zhang: "Landau damping of quantum plasmons in metal nanostructures". *New Journal of Physics* 2013, **15**:023011.
11. V. G. Hartland: "Optical Studies of Dynamics in Noble Metal Nanostructures". *Chemical Reviews* 2011, **111**:3858-3887.
12. B. Foerster, V. A. Spata, E. A. Carter, C. Sönnichsen, S. Link: "Plasmon damping depends on the chemical nature of the nanoparticle interface". *Science Advances* 2019, **5**:eaav0704.
13. S. Link, M. A. El-Sayed: "Optical Properties and Ultrafast Dynamics of Metallic Nanocrystals". *Annual Review of Physical Chemistry* 2003, **54**:331-366.
14. M. B. Mohamed, T. S. Ahmadi, S. Link, M. Braun, M. A. El-Sayed: "Hot electron and phonon dynamics of gold nanoparticles embedded in a gel matrix". *Chemical Physics Letters* 2001, **343**:55-63.
15. H. Tang, C.-J. Chen, Z. Huang, J. Bright, G. Meng, R.-S. Liu, N. Wu: "Plasmonic hot electrons for sensing, photodetection, and solar energy applications: A perspective". *The Journal of Chemical Physics* 2020, **152**:220901.
16. J. A. Schuller, E. S. Barnard, W. Cai, Y. C. Jun, J. S. White, M. L. Brongersma: "Plasmonics for extreme light concentration and manipulation". *Nature Materials* 2010, **9**:193-204.
17. K. Wu, J. Chen, J. R. McBride, T. Lian: "Efficient hot-electron transfer by a plasmon-induced interfacial charge-transfer transition". *Science* 2015, **349**:632-635.
18. A. Furube, S. Hashimoto: "Insight into plasmonic hot-electron transfer and plasmon molecular drive: new dimensions in energy conversion and nanofabrication". *npg asia materials* 2017, **9**:e454.
19. A. Furube, L. Du, K. Hara, R. Katoh, M. Tachiya: "Ultrafast Plasmon-Induced Electron Transfer from Gold Nanodots into TiO₂ Nanoparticles". *Journal of the American Chemical Society* 2007, **129**:14852-14853.
20. M. S. Devadas, K. Kwak, J.-W. Park, J.-H. Choi, C.-H. Jun, E. Sinn, G. Ramakrishna, D. Lee: "Directional Electron Transfer in Chromophore-Labeled Quantum-Sized Au₂₅ Clusters: Au₂₅ as an Electron Donor". *The Journal of Physical Chemistry Letters* 2010, **1**:1497-1503.
21. J. Cheng, Y. Li, M. Plissonneau, J. Li, J. Li, R. Chen, Z. Tang, L. Pautrot-d'Alençon, T. He, M. Tréguer-Delapierre *et al.*: "Plasmon-induced hot electron transfer in AgNW@TiO₂@AuNPs nanostructures". *Scientific Reports* 2018, **8**:14136.
22. S. K. Cushing, J. Li, F. Meng, T. R. Senty, S. Suri, M. Zhi, M. Li, A. D. Bristow, N. Wu: "Photocatalytic Activity Enhanced by Plasmonic Resonant Energy Transfer from Metal to Semiconductor". *Journal of the American Chemical Society* 2012, **134**:15033-15041.
23. T. E. Tesema, B. Kafle, T. G. Habteyes: "Plasmon-Driven Reaction Mechanisms: Hot Electron Transfer versus Plasmon-Pumped Adsorbate Excitation". *The Journal of Physical Chemistry C* 2019, **123**:8469-8483.
24. C. Boerigter, R. Campana, M. Morabito, S. Linic: "Evidence and implications of direct charge excitation as the dominant mechanism in plasmon-mediated photocatalysis". *Nature Communications* 2016, **7**:10545.
25. C. Boerigter, U. Aslam, S. Linic: "Mechanism of Charge Transfer from Plasmonic Nanostructures to Chemically Attached Materials". *ACS Nano* 2016, **10**:6108-6115.
26. W.-Y. Rho, D. H. Song, H.-Y. Yang, H.-S. Kim, B. S. Son, J. S. Suh, B.-H. Jun: "Recent advances in plasmonic dye-sensitized solar cells". *Journal of Solid State Chemistry* 2018, **258**:271-282.

27. Z. Eroglu, O. Comegys, L. Quintanar, N. Azam, S. Elafandi, M. Mahjouri-Samani, A. Boulesbaa: "Ultrafast dynamics of exciton formation and decay in two-dimensional tungsten disulfide (2D-WS₂) monolayers". *Physical Chemistry Chemical Physics* 2020, **22**:17385-17393.
28. Z. E. Eroglu, D. Contreras, P. Bahrami, N. Azam, M. Mahjouri-Samani, A. Boulesbaa: "Filling Exciton Trap-States in Two-Dimensional Tungsten Disulfide (WS₂) and Diselenide (WSe₂) Monolayers". *Nanomaterials* 2021, **11**(3):770.
29. J.-S. Shen, T. Yu, J.-W. Xie, Y.-B. Jiang: "Photoluminescence of CdTe nanocrystals modulated by methylene blue and DNA. A label-free luminescent signaling nanohybrid platform". *Physical Chemistry Chemical Physics* 2009, **11**:5062–5069.
30. J. Schlenkrich, D. Zámbo, A. Schlosser, P. Rusch, N. C. Bigall: "Revealing the Effect of Nanoscopic Design on the Charge Carrier Separation Processes in Semiconductor-Metal Nanoparticle Gel Networks". *Advanced Optical Materials* 2022, **10**:2101712.
31. T. Kiyonaga, M. Fujii, T. Akita, H. Kobayashi, H. Tada: "Size-dependence of Fermi energy of gold nanoparticles loaded on titanium(IV) dioxide at photostationary state". *Physical Chemistry Chemical Physics* 2008, **10**:6553–6561.
32. A. Fernández-Pérez, G. Marbán: "Visible Light Spectroscopic Analysis of Methylene Blue in Water; What Comes after Dimer?". *ACS Omega* 2020, **5**(46):29801-29815.
33. A. Fernández-Pérez, T. Valdés-Solís, G. Marbán: "Visible light spectroscopic analysis of Methylene Blue in water; the resonance virtual equilibrium hypothesis". *Dyes and Pigments* 2019, **161**:448-456.
34. J. C. Dean, S. Rafiq, D. G. Oblinsky, E. Cassette, C. C. Jumper, G. D. Scholes: "Broadband Transient Absorption and Two-Dimensional Electronic Spectroscopy of Methylene Blue". *The Journal of Physical Chemistry A* 2015, **119**:9098-9108.
35. A. Boulesbaa, Z. Huang, D. Wu, T. Lian: "Competition between Energy and Electron Transfer from CdSe QDs to Adsorbed Rhodamine B". *The Journal of Physical Chemistry C* 2010, **114**:962-969.
36. M. Trejo-Valdez, R. Torres-Martínez, N. Peréa-López, P. Santiago-Jacinto, C. Torres-Torres: "Contribution of the Two-Photon Absorption to the Third Order Nonlinearity of Au Nanoparticles Embedded in TiO₂ Films and in Ethanol Suspension". *The Journal of Physical Chemistry C* 2010, **114**:10108–10113.
37. D. Severino, H. C. Junqueira, M. Gugliotti, D. S. Gabrielli, M. S. Baptista: "Influence of Negatively Charged Interfaces on the Ground and Excited State Properties of Methylene Blue". *Photochemistry and Photobiology* 2003, **77**(5):459-468.
38. A. Rakovich, Y. P. Rakovich, J. F. Donegan: "Optical Studies of the Methylene Blue-Semiconductor Nanocrystals Hybrid System". *e-Journal of Surface Science and Nanotechnology* 2009, **7**:349-353.
39. Y. Tang, Z. Jiang, G. Xing, A. Li, P. D. Kanhere, Y. Zhang, T. C. Sum, S. Li, X. Chen, Z. Dong: "Efficient Ag@ AgCl cubic cage photocatalysts profit from ultrafast plasmon-induced electron transfer processes". *Advanced Functional Materials* 2013, **23**:2932–2940.
40. J. Chen, T. C. Cesario, P. M. Rentzepis: "Time resolved spectroscopic studies of methylene blue and phenothiazine derivatives used for bacteria inactivation". *Chemical Physics Letters* 2010, **498**:81-85.
41. J. Kadokawa, H. Izawa, T. Ohta, S. Wakizono, K. Yamamoto: "Photo-Induced Reduction Reaction of Methylene Blue in an Ionic Liquid". *International Journal of Organic Chemistry* 2011, **1**:158-161.